Article

A Comparison of Empirical Procedures for Fatigue Damage Prediction in Instrumented Risers undergoing Vortex-Induced Vibration

Chen Shi [1,†*], Lance Manuel [2] and Michael Tognarelli [3]

[1] China University of Petroleum (East China); shichen2004@hotmail.com
[2] University of Texas; lmanuel@mail.utexas.edu
[3] BP America Production Co.; Michael.Tognarelli@bp.com
* Correspondence: shichen2004@hotmail.com; Tel.: +86-156-2102-0406
† Current address: 66 Changjiang Xi Rd., Qingdao, Shandong, China 266580

Version September 21, 2018 submitted to Preprints

Abstract: To gain insight into riser motions and associated fatigue damage due to vortex-induced vibration (VIV), data loggers such as strain sensors and/or accelerometers are sometimes deployed on risers to monitor their motion in different current velocity conditions. Accurate reconstruction of the riser response and empirical estimation of fatigue damage rates over the entire riser length using measurements from a limited number of sensors can help in efficient utilization of the costly measurements recorded. Several different empirical procedures are described here for analysis of the VIV response of a long flexible cylinder subjected to uniform and sheared current profiles. The methods include weighted waveform analysis (WWA), proper orthogonal decomposition (POD), modal phase reconstruction (MPR), a modified WWA procedure, and a hybrid method which combines MPR and the modified WWA method. Fatigue damage rates estimated using these different empirical methods are compared and cross-validated against measurements. Detailed formulations for each method are presented and discussed with examples. Results suggest that all the empirical methods, despite different underlying assumptions in each of them, can be employed to estimate fatigue damage rates quite well from limited strain measurements.

Keywords: riser; vortex-induced vibration; fatigue damage prediction, empirical method

1. INTRODUCTION

Current velocity flow fields on marine risers can lead to the formation and shedding of vortices downstream; fluctuations in resulting hydrodynamic pressures can cause such risers to experience sustained vortex-induced vibration (VIV), which can lead to fatigue damage. Accumulated fatigue damage may cause riser failure, a shortened service life, and even ocean pollution. To prevent such catastrophic consequences, it is useful to be able to accurately estimate the rate of fatigue damage accumulation and the expected service life of a marine riser at the design stage, or to measure and monitor the accumulated fatigue damage and the remaining life for an installed riser. In an effort to achieve this ambitious goal, several marine riser monitoring campaigns have been undertaken over the past decade [1]. Riser responses (such as strains and/or accelerations) are measured at discrete locations along the riser's axis. Often, ocean currents are also measured at a nearby location over the period of the riser monitoring campaign. Such in-situ full-scale measurements of riser VIV response are extremely valuable in the study of riser VIV response and the estimation of fatigue damages.

In contrast to the use of riser response measurement campaigns, given a current profile and the physical properties of a riser, the response and fatigue damage rate of the riser may be estimated using available semi-empirical computer programs. The estimated riser response, though, with many of these tools, only contains energy of the first harmonic at the Strouhal frequency (vortex-shedding frequency) while neglecting or filtering out higher harmonics (i.e., the response at frequencies that are multiples of the Strouhal frequency) that can result in fatigue damage rate underestimated by a factor

 doi:10.20944/preprints201809.0426.v1

as large as 40 [2]. Some recent studies have presented approaches to incorporate higher harmonics in fatigue damage estimation (see, for example, Jhingran and Vandiver [3] and Modarres-Sadeghi et al. [4]). The general idea is to estimate the ratio of the higher harmonics to the first harmonic from the recorded riser response, and then to use that ratio to modify the estimated fatigue damage rate caused by the first harmonic alone. In addition to the semi-empirical computer programs, numerical simulation in computational fluid dynamics (CFD) is an alternative approach used to assess the VIV response of marine risers. For example, Meneghini et al. [5] and Yamamoto et al. [6] simulate the vortex-induced vibration of a flexible cylinder using two-dimensional Discrete Vortex Method (DVM). Huang et al. [7] predict the VIV response of a flexible cylinder using an unsteady, three-dimensional Reynolds-averaged Navier-Stokes (RANS) method. Despite dramatic progress in the application of CFD for riser VIV analysis, a complete three-dimensional numerical simulation for risers at realistic flow field is still prohibitive due to the overwhelming complexity and the intensive computational requirements.

In the present study, several empirical methods are employed to estimate VIV response and fatigue damage rates over the entire length of a riser using riser responses measured at several discrete locations. Unlike semi-empirical or analytical VIV prediction software, empirical methods only require data (i.e., the measured riser response); none (or few) information on the current profile, physical and hydrodynamic properties of the riser are required. Five empirical methods, referred to as WWA (Weighted Waveform Analysis), modified WWA, POD (Proper Orthogonal Decomposition), MPR (Modal Phase Reconstruction), and a hybrid method which combines MPR and modified WWA, are studied. Four data sets of the Norwegian Deepwater Programme (NDP), which were obtained from tests on a densely instrumented model riser, are employed to test and compare the different methods. Riser response and fatigue damage rates over the entire riser length are estimated using strain measurements from a limited number of sensors. The mathematical formulation and basis for each method is briefly presented in Section 3; as well, underlying assumptions, advantages, and disadvantages of each method are discussed with examples. By comparing the estimated riser response and fatigue damage rates at selected locations with those obtained directly from the measurements, it is found that all the empirical methods discussed, despite the different underlying assumptions in each of them, may be employed to estimate fatigue damage rates quite well from limited measurements.

2. MODEL RISER AND DATA SETS

The NDP model riser experiment was carried out by the Norwegian Marine Technology Research Institute (Marintek) in 2003, by horizontally towing a flexible cylinder in the Ocean Basin test facility. The experimental setup is schematically plotted as in Fig. 1, which shows that a horizonal cylinder is attached to the test rig and towed by the crane and gondola. Towing both ends of the cylinder at the same speed by the crane in one direction simulates a uniform current flow; while, with one end fixed and towing the other end using the gondola to traverse a circular arc simulates a linearly sheared current flow. The maximum towing speed is 2.4 m/s which simulates the flow field of the Reynolds number about 70,000. The key physical and hydrodynamic properties of the model cylinder are listed in Table 1. More details related to the design and setup of the experiment may be found in references of Trim et al. [8], and Braaten and Lie [9]. Riser responses were measured using 24 strain sensors (one sensor failed for some test runs; hence, in some cases, only 23 strain sensors were available) and 8 accelerometers for the cross-flow (CF) direction; similarly, in the inline (IL) direction, measurements from 40 strain sensors and 8 accelerometers were available.

Among the six data sets available at the VIV data repository [10], four of them were obtained from tests on bare/unstraked risers. Table 2 summarizes current characteristics, root-mean-square (RMS) values of the CF displacement (normalized to the outer diameter of the cylinder cross-section, D), and the time duration of each data set. The durations vary from about 18 sec. to 60 sec., which ensure over 100 cycles of the CF oscillations for each data set. Because of the large RMS values of the CF displacement, the riser response is thought to be associated with VIV and, as such, these four

Preprints (www.preprints.org) | NOT PEER-REVIEWED | Posted: 21 September 2018 doi:10.20944/preprints201809.0426.v1

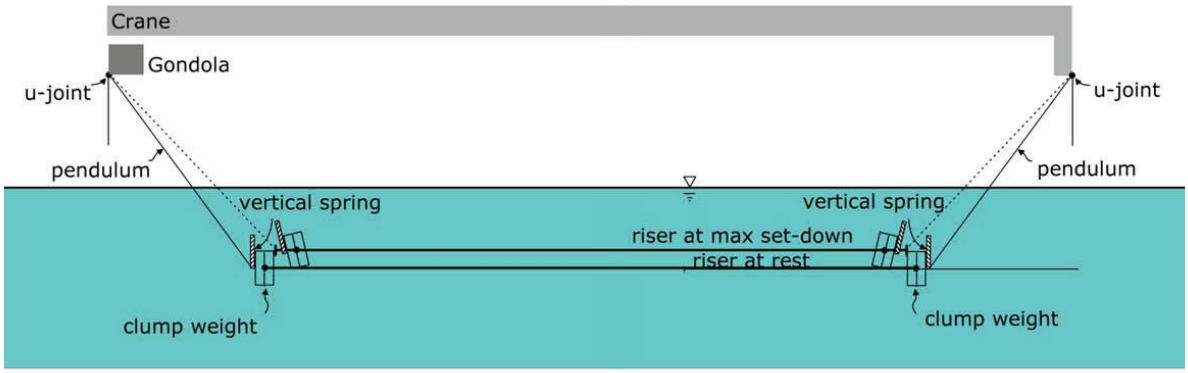

(a)

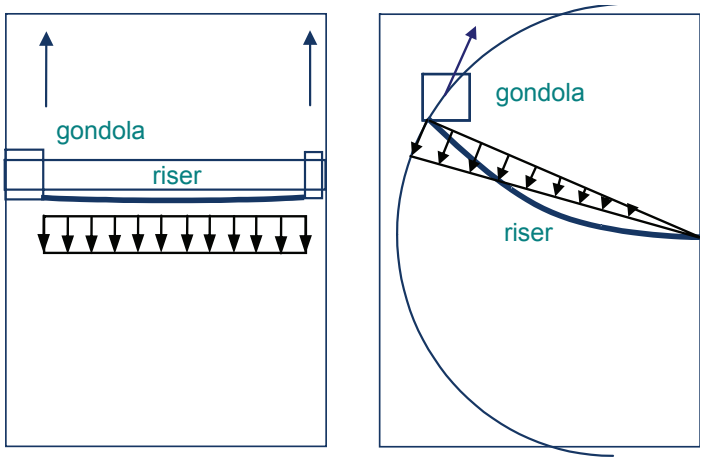

(b)

Figure 1: Schematics of the experimental setup: (a) test rig in vertical view; and (b) simulated current profiles in plan view, left is uniform current flow and right is linearly sheared current flow [8].

Table 1: Physical and hydrodynamic properties of the NDP model riser.

Length (m)	38
Outer diameter (mm)	27
Wall thickness (mm)	3
Mass of riser per unit length (kg/m)	0.933
Mass of displaced water per unit length (kg/m)	0.576
Mean effective tension (N)	4000 to 6000
Bending stiffness (N-m^2)	598.8
Maximum Reynolds number	~70,000

tests are well suited for this study. Note that, in Table 2, the RMS values of the CF displacement are calculated based on the entire length of record and the largest value from all the eight accelerometers was reported.

Given CF and IL measurements at the same cross-section of a riser, Baarholm et al. [11] computed the fatigue damage at several points along the outer circumference, and noted that the maximum fatigue damage for that cross-section location was usually equal to the larger of the CF fatigue damage and the IL fatigue damage. For the four NDP data sets, fatigue damage rates (per year) at locations of the twenty-four CF strain sensors and the forty IL strain sensors are calculated and illustrated in Fig. 2. It is seen that the fatigue damage rates in the CF direction are almost always larger than that in the IL

Preprints (www.preprints.org) | NOT PEER-REVIEWED | Posted: 21 September 2018 doi:10.20944/preprints201809.0426.v1

direction; this suggests that the fatigue life is largely controlled by the CF fatigue damage. Hence, in this study, only the CF responses and fatigue damages are considered.

Table 2: The four bare riser NDP data sets.

Event no.	Current profile	Max. current speed (m/s)	Largest RMS CF-disp./D	Duration (s)
2120	Uniform	1.4	0.44	25
2150	Uniform	1.7	0.40	18
2350	Sheared	0.7	0.42	60
2420	Sheared	1.4	0.37	27

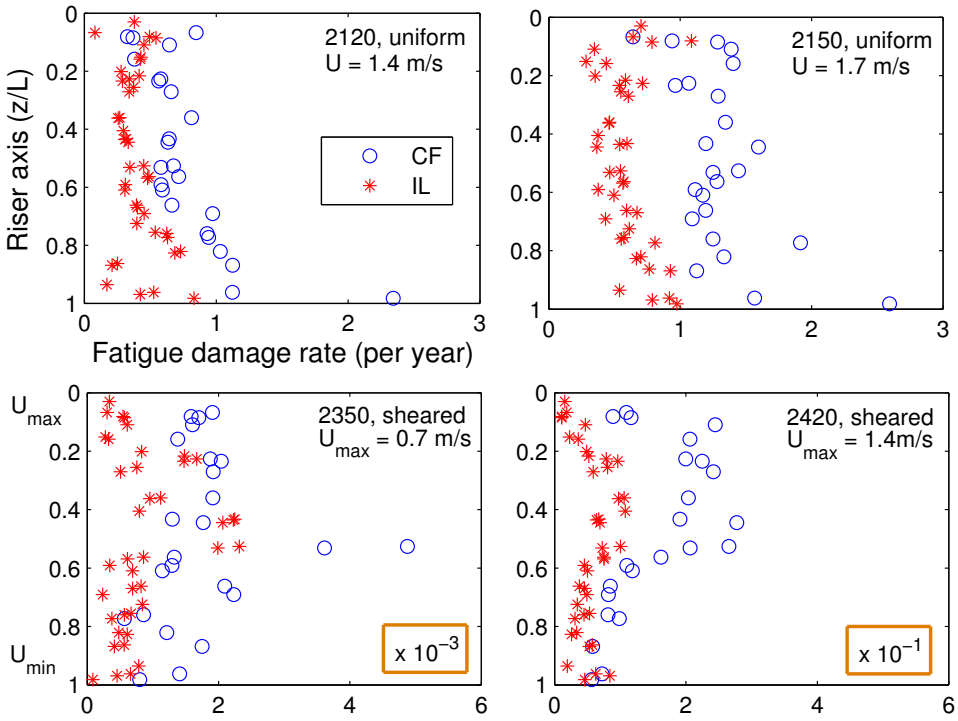

Figure 2: Measured CF and IL fatigue damage rates (per year) of the four NDP data sets.

3. EMPIRICAL FATIGUE DAMAGE ESTIMATION

The densely instrumented NDP model riser (with twenty-four strain sensors in the CF direction) allows us to test different empirical methods by use of cross-validation where estimations are compared to measurements as follows. First, select any one sensor (among the original twenty-four sensors) as the "target" sensor and use the remaining twenty-three sensors as "input" sensors; use the empirical method under consideration along with measurements from the input sensors to estimate strain time series at the location of the target sensor. Next, assess the fatigue damage rate at the location of the target sensor from the estimated strain and compare it with the true value, which was computed directly from the strain measured by the target sensor (but never used in estimation by the empirical method). The process is iterated by selecting a different target sensor each time until all the twenty-four sensors have been selected. These iterative steps are followed for each empirical method. A single parameter, the Damage Ratio (DR), defined as the ratio of the estimated fatigue damage to the true fatigue damage at the target sensor, is used as an indicator of the "quality" of the empirical method.

Preprints (www.preprints.org) | NOT PEER-REVIEWED | Posted: 21 September 2018 doi:10.20944/preprints201809.0426.v1

The cumulative fatigue damage can be estimated using stress time series, which equal to the strain time series multiplied with the Young's modulus of the riser material, using Miner's rule [12], the rainflow cycle-counting algorithm (details may be found in literatures such as [13] and [14]), and S-N curve approach, and is expressed as:

$$d = \frac{n}{N} = \frac{n}{aS^{-b}} \tag{1}$$

where d is the cumulative fatigue damage caused by the given stress/strain time series. S and n are the equivalent stress range and the number of cycles, respectively, estimated by use of the rainflow cycle-counting algorithm. N is the number of cycles to fatigue failure at the stress range S. In this study, F2 S-N curve with parameters $a = 4.266 \times 10^{11}$ and $b = 3.0$ is adopted [15].

The damage ratio (DR) which is used to evaluate the empirical method is then calculated as:

$$DR = \frac{d_e}{d_t} = \frac{n_e S_e^b}{n_t S_t^b} \tag{2}$$

where the estimated fatigue damage, d_e, the estimated stress range, S_e, and the estimated number of cycles, n_e, are calculated based on the estimated/reconstructed stress time series. Similarly, d_t, S_t, and n_t are the fatigue damage, stress range, and number of cycles calculated based on the true/measured stress time series at the same location. As illustrated in Eqs. 1 and 2, the fatigue damage is proportional to the b^{th} (usually $b = 3$ or 4) power of the amplitude of the stress/strain and, thus, the damage ratio is more critical to the error of the reconstructed riser response compared with the ratios directly based on the strain or displacement (e.g. the ratio of the RMS values of the strain or the amplitude). This is the main reason of choosing the ratio of fatigue damage instead of other scalars, such as the ratio of RMS values of strains (strain-RMS ratio) or the ratio of RMS values of displacements (displacement-RMS ratio), to evaluate the empirical methods. An example presented in Section 4 will be used to demonstrate this discussion.

In this section, the theoretical formulation for each empirical method is presented very briefly. Then, using the NDP2350 (sheared current) data set for illustration and making use of strain sensor no. 4 at the location of $z/L = 0.11$ (z is the spatial coordinate along the riser axis and L is the riser length) as the target sensor, key points including advantages and disadvantages of each method are highlighted. In sections 4 and 5, fatigue damage rates estimated by use of different empirical methods at various locations (including the location of sensor no. 4) for all the four NDP data sets are presented. Based on these results, the advantages and disadvantages of each empirical method, and some basic guidelines of how to select the most appropriate empirical method to suit a specific situation are discussed in sections 7 and 8.

3.1. Weighted Waveform Analysis

Weighted Waveform Analysis (WWA) is a computational procedure that is widely used to analyze and reconstruct the response over the entire length of a riser from measurements at a limited number of sensors [8], [16].

Assume that the riser displacement, x, at location, z, and time, t, may be expressed approximately as a weighted sum of N assumed modes:

$$x(z,t) = \sum_{i=1}^{N} w_i(t)\varphi_i(z) \tag{3}$$

where it is assumed that by selecting N (not necessarily consecutive) modes, one can represent the riser displacement at any location, z. Also, $\varphi_i(z)$ represents the n_i^{th} mode shape of the displacement, while $w_i(t)$ represents the time-varying modal weight to be applied with the n_i^{th} mode shape. Note that, $i = 1, 2, \ldots, N$, is associated with the selected mode set which include the n_1^{th}, n_2^{th}, ..., and n_N^{th}

Preprints (www.preprints.org) | NOT PEER-REVIEWED | Posted: 21 September 2018 doi:10.20944/preprints201809.0426.v1

mode; and these selected modes are not necessarily to be sequentially ordered. Also, the "mode" in the empirical methods discussed here, means a deformed shape of the riser associated with dominant energy in the power spectral density (PSD) of the CF strain at the logger locations.

The bending strain, which equals the product of the riser outer radius, R, and the local curvature, x'', may be expressed as follows:

$$\varepsilon(z,t) = Rx''(z,t) = \sum_{i=1}^{N} Rw_i(t)\varphi_i''(z) \tag{4}$$

For the NDP model riser of a constant tension and pinned-pinned boundary conditions, it is assumed that the mode shapes are represented as sinusoidal functions:

$$\varphi_i(z) = \sin\left(\frac{n_i\pi z}{L}\right); \quad \varphi_i''(z) = -\left(\frac{n_i\pi}{L}\right)^2 \sin\left(\frac{n_i\pi z}{L}\right) \tag{5}$$

where $\varphi_i(z)$ and $\varphi_i''(z)$ are the n_i^{th} mode shape of the displacement and curvature, respectively, and L is the riser length.

Given strain measurements or, equivalently, curvature measurements at M logger locations, z_j (where $j = 1$ to M), WWA requires solution of a system of equations in matrix form:

$$\mathbf{Aw} = \mathbf{d} \tag{6}$$

where the $M \times N$ matrix, $\mathbf{A}$, comprises curvatures of the assumed mode shapes at all the logger locations and the vector, $\mathbf{d}$, represents riser curvatures and is formed from the measured strains at all loggers—i.e., $A_{j,i} = \varphi_i''(z_j)$ and $d_j = \varepsilon_j(t)/R = \varepsilon(z_j,t)/R$. Equation 6 is a linear system of M equations with N weights ($\mathbf{w}^T = \{w_1, w_2, \ldots w_N\}$) need to estimated. At any instant of time, t, as long as $N \leq M$, the modal weights vector, $\mathbf{w}$, may be solved for in a least squares sense:

$$\mathbf{w}(t) = \left(\mathbf{A}^T\mathbf{A}\right)^{-1}\mathbf{A}^T\mathbf{d}(t) \tag{7}$$

In the present study, where twenty-three strain sensors are available, it is found that careful selection of the modes based on frequencies corresponding to peaks in the CF strain power spectra, generally, provides good WWA-based reconstructed strain time series at target sensors. In our studies, twelve mode (i.e., $N = 12$) was generally a good choice. The procedure for the selection of the N modes is important, and it is briefly described next.

Given the CF strain time series, $\varepsilon(z_j,t)$, measured at each of the twenty-three locations, z_j (where $j = 1,2,3,5,\ldots,24$; i.e., assume that the target sensor no. 4 does not exist), its power spectral density (PSD), $PSD_j(f)$, describes the energy distribution by frequency of the riser response at that location. As illustrated in Fig. 3(a), the twenty-three input strain power spectra indicate very similar frequency content; all these spectra show the presence of the first and third harmonics in the response (the fifth harmonic is also visible if the PSDs were plotted on log scale). The summation of the PSDs at each frequency for all the twenty-three sensors, i.e., $\sum_j PSD_j(f)$ (see Fig. 3(b)) is assumed to account for the energy distribution by frequency over the entire riser and is, therefore, used for the WWA mode selection. First, the twelve separate peaks which have highest spectral values are identified. As illustrated in Fig. 3(b), the selected peaks cover the first, third and fifth harmonics as well as the second and fourth harmonics of the input signals. Second, the associated mode numbers are determined by comparing these peak frequencies with the estimated natural frequencies of the riser. The riser is assumed to be dominated by tensioned-string behavior and its bending stiffness is assumed to be

Preprints (www.preprints.org) | NOT PEER-REVIEWED | Posted: 21 September 2018 doi:10.20944/preprints201809.0426.v1

negligible. Note that the riser's natural frequencies are calculated from the physical properties of the riser and an assumed added mass coefficient using:

$$f_n = \frac{n}{2L}\sqrt{\frac{T}{m + C_a m_w}} \tag{8}$$

where f_n is the n^{th} natural frequency of the riser, L is the riser length, T is the tension in the riser, m is the mass of the riser per unit length, m_w is the mass of the displaced water per unit length, and C_a is the added mass coefficient. The added mass coefficient is one of the least understood hydrodynamic properties associated with riser VIV; its value is a function of the vibration amplitude and the current flow speed. For simplicity, in this study, it is assumed that $C_a = 0$ for uniform current profiles, and $C_a = 1.0$ for sheared current profiles (this simplifying assumption is based on the propagation speed of traveling waves observed on the available NDP riser data sets).

Using the WWA procedure, strain time series at locations over the entire length of the riser, including at the location of the target sensor, may be reconstructed based on Eq. 4. Figure 3(c) compares the energy distribution by frequency in the reconstructed CF strain PSD at sensor no. 4 (dashed red line) with the CF strain PSD obtained directly from measurements (solid blue line) at the location of the target sensor; the comparison suggests that the first and higher harmonics are reasonably well represented by application of the WWA procedure. Based on the assumed mode shapes, the response over the entire length of the riser may be reconstructed after obtaining the time-varying modal weights. Figure 3(d) presents RMS curvature values at the location of the twenty-four sensors based on measurements; the blue circles indicate these values at the twenty-three input sensors, and the red cross indicates the value at the target sensor. The solid line indicates the corresponding RMS curvature estimated by the WWA procedure. The results suggest that the reconstructed curvatures reflect the presence of the first and higher harmonics and that these reconstructed curvatures match measured values reasonably well at all the sensor locations.

The fatigue damage ratio, representing the ratio of the estimated damage to that based directly on measurements, at the target sensor (i.e., sensor no. 4), is 1.47, which suggests that the fatigue damage is overestimated by a factor of 1.47 by the WWA method. Similar results for other choices of the target sensor are discussed in Section 4.

In another study by the authors [17], the WWA method was incorporated with a data-driven mode identification algorithm, where the natural frequency of a riser was empirically estimated using the measured riser's responses and temporal and spatial frequency analysis techniques. The empirically estimated natural frequency of the NDP model riser is close to the value assumed in this study, which is calculated using the riser's physical properties, and, thus, the two WWA-based response reconstruction methods generate fatigue damage ratios of comparable accuracy. More details can be found in the work of Shi et al. [17].

3.2. Modified Weighted Waveform Analysis

By introducing cosine terms to complement the sine terms for each frequency component in the WWA method, a modified WWA procedure results that can better account for the effect of traveling waves in the riser response as well as for local curvature changes at boundaries and other discontinuities. In lieu of Eq. 3, we now have:

$$\begin{aligned} x(z,t) &= \sum_{i=1}^{N} \left[a_i(t)\varphi_i(z) + b_i(t)\psi_i(z)\right] \\ \varphi_i(z) &= \sin\left(\frac{n_i \pi z}{L}\right); \psi_i(z) = \cos\left(\frac{n_i \pi z}{L}\right) \end{aligned} \tag{9}$$

where $a_i(t)$ and $b_i(t)$ are modal weights associated with assumed sine and cosine mode shapes, $\varphi_i(z)$ and $\psi_i(z)$, respectively. Strains are computed in a similar manner as with the WWA method.

Preprints (www.preprints.org) | NOT PEER-REVIEWED | Posted: 21 September 2018 doi:10.20944/preprints201809.0426.v1

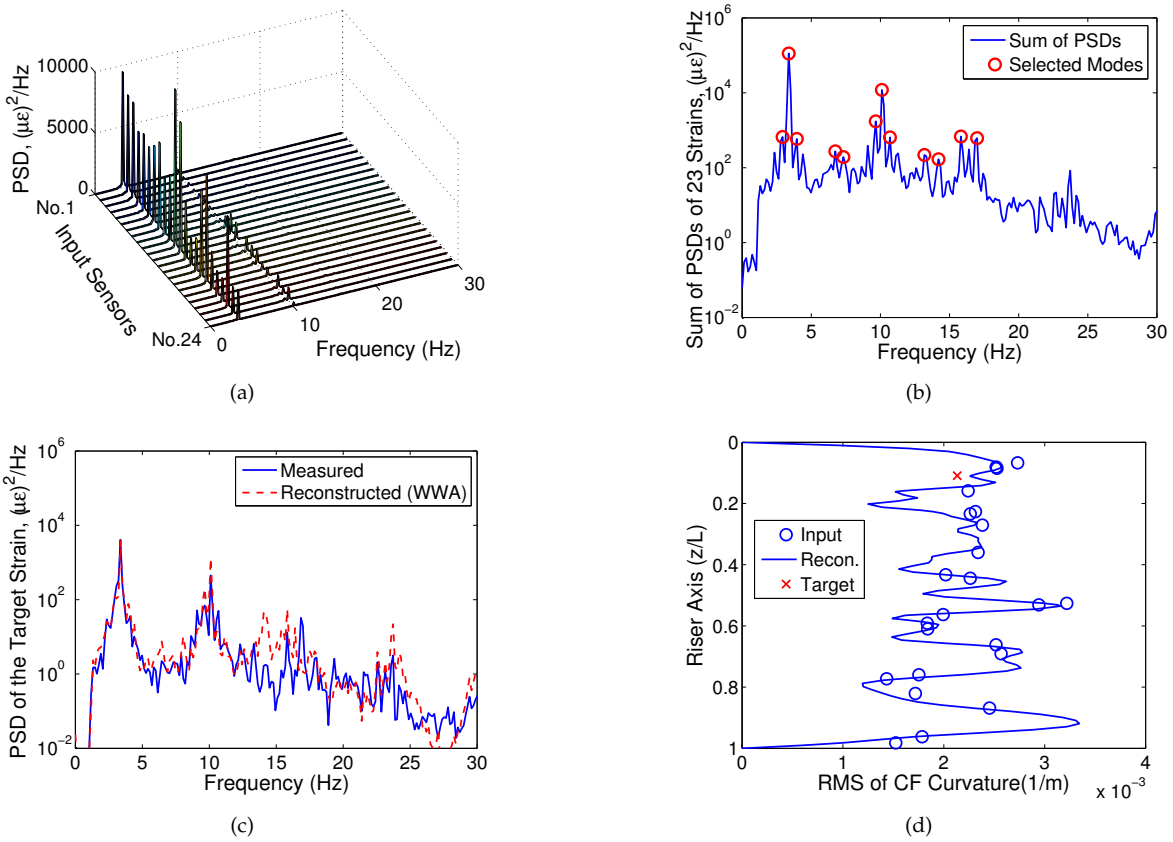

Figure 3: The WWA procedure applied with twenty-three input sensors (sensor no. 4 is the target) for the NDP2350 (sheared current) data set: (a) PSDs of the strains measured at the twenty-three sensors; (b) Summation of the strain PSDs at each frequency and identification of the selected modes; (c) Strain PSD at the target sensor, reconstructed vs. measured; and (d) RMS curvatures, reconstructed vs. measured.

As with the WWA procedure, given curvature measurements at M logger locations, a system of equations in matrix form results (exactly as in Eq. 6), but with modified terms—i.e., $A_{j,2i-1} = \varphi_i''(z_j)$ and $A_{j,2i} = \psi_i''(z_j)$. This is a linear system of M equations with $2N$ weights to be estimated. At any instant of time, t, as long as $2N \leq M$, the modal weights, ($\mathbf{w}^T = \{a_1, b_1, a_2, b_2 \ldots a_N, b_N\}$), may again be solved for in a least squares sense using Eq. 7. The riser response such as CF bending strain, at any location, z, may then be reconstructed. Though the modified WWA procedure can better describe traveling waves in the riser response as well as local curvature variations (than is possible with the WWA method), the smaller number of modes that may be assumed given the same suite of measurements represents a tradeoff.

It should be noted that the modified WWA procedure presented here is similar to the spatial Fourier decomposition with the "full reconstruction criterion" that is employed by Mukundan [18], [19]; however, one key difference is that the those studies use sequentially ordered modes, while the modified WWA method is based on selection of important physically excited (energetic) modes that are not, in general, sequential.

With the modified WWA method, where twenty-three input strain sensors are available (i.e., M=23), careful selection of six modes (i.e., N=6) based on generally non-consecutive frequencies corresponding to peaks in the CF strain power spectra provided reconstructed strain time series with reasonable accuracy. Figure 4 presents results for the modified WWA method which are analogous to those presented for the WWA method in Fig. 3. The PSD for CF strain at each input logger and the summation of all these PSDs at each frequency are plotted in Figs. 4(a) and 4(b), respectively. The six

Preprints (www.preprints.org) | NOT PEER-REVIEWED | Posted: 21 September 2018 doi:10.20944/preprints201809.0426.v1

modes selected in a similar manner to the procedure used with the WWA method, include from the first to the fifth harmonics of the input signals. Results summarizing the reconstructed CF strain PSD and the reconstructed RMS curvature at the locations of the various sensors are presented in Figs. 4(c) and 4(d), respectively. The results suggest that at the target sensor, the PSD of the reconstructed CF strain matches the corresponding PSD based on actual strain measurements quite well; also, the RMS values of the reconstructed curvatures match measured values reasonably well at all the sensor locations.

The fatigue damage ratio, representing the ratio of the estimated damage to that based directly on measurements, at the target sensor (i.e., sensor no. 4), is 1.62, which suggests that the fatigue damage is overestimated by 62% by the modified WWA method. Similar results for other choices of the target sensor are discussed in Section 4.

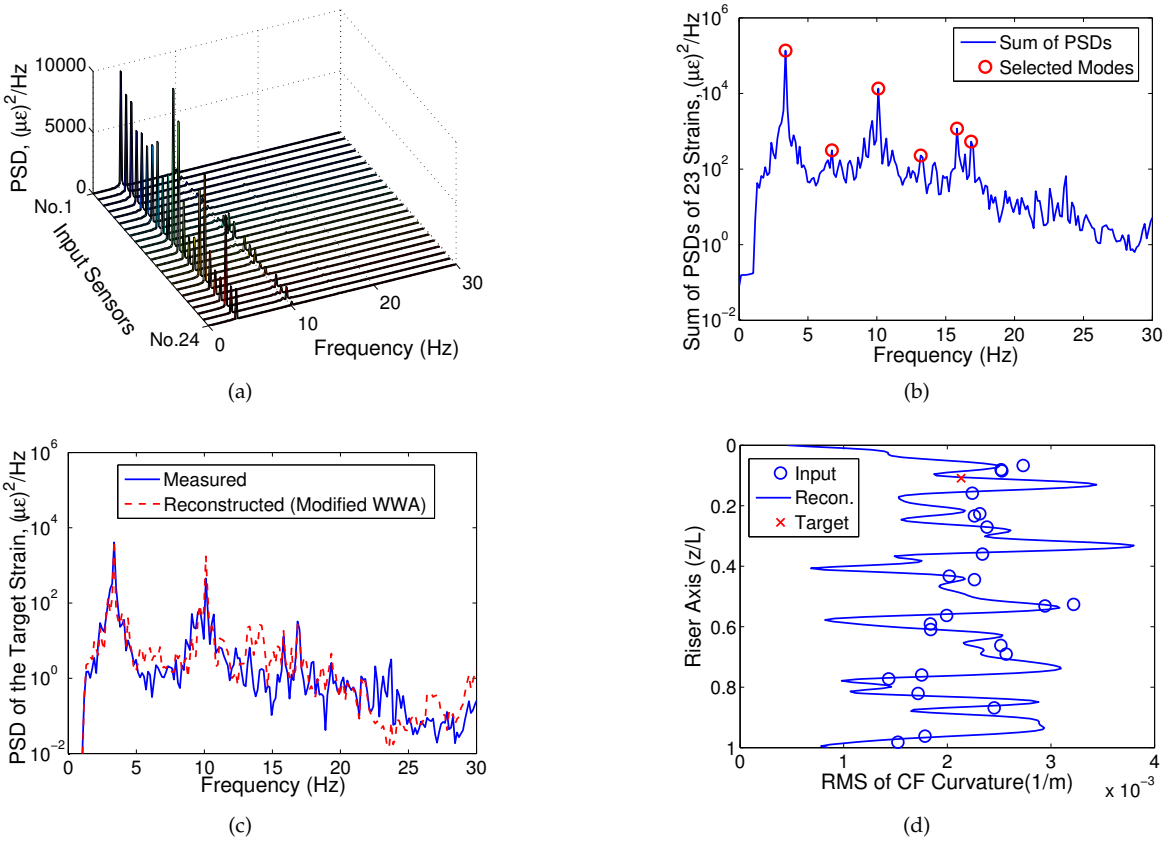

Figure 4: The modified WWA procedure applied with twenty-three input sensors (sensor no. 4 is the target) for the NDP2350 (sheared current) data set: (a) PSDs of the strains measured at the twenty-three sensors; (b) Summation of the strain PSDs at each frequency and identification of the selected modes; (c) Strain PSD at the target sensor, reconstructed vs. measured; and (d) RMS curvatures, reconstructed vs. measured.

3.3. Proper Orthogonal Decomposition

The WWA approach presented requires a priori assumed mode shapes based on knowledge of the physical properties of the riser; the modified WWA approach is directly related to these modes by introducing cosine function counterparts to each sine function. For the NDP model riser, the mass and tension force are almost constant along its length; hence, it might be reasonable to assume sinusoidal functions for the mode shapes as was done with the WWA method used in this study. For real drilling risers, the mass and the tension force often vary spatially due, for example, to the presence of buoyancy

Preprints (www.preprints.org) | NOT PEER-REVIEWED | Posted: 21 September 2018 doi:10.20944/preprints201809.0426.v1

units. In such cases, riser mode shapes will usually deviate from simple sinusoidal functions and can be difficult to estimate accurately. The error in assumed mode shapes affects the accuracy of approaches such as the WWA method and in resulting estimations of response and fatigue damage.

In the following, Proper Orthogonal Decomposition (POD) is proposed as an alternative empirical procedure for riser VIV response and fatigue analysis. With POD, empirical mode shapes are estimated from the data alone and do not rely on assumed mode shapes nor on knowledge of the physical properties of the riser. POD is useful for extracting energetic spatial "modes" or patterns of variation of any physical phenomenon that is represented by a high-dimensional spatio-temporal stochastic field (such as the suite of riser strain time series from multiple sensors that we have here). The application of POD for the analysis of riser VIV response may be found in the literature (see, for example, Kleiven [20] or Srivilairit and Manuel [21]).

Given a suite of strain time series measured at M locations, $\mathbf{V}(t) = \{v_1(t), v_2(t), \ldots, v_M(t)\}^T$, one can establish a $M \times M$ covariance matrix, $\mathbf{C}_v$, from the strain time series, $\mathbf{V}(t)$. By solving an eigenvalue problem, one can diagonalize $\mathbf{C}_v$ so as to obtain the matrix, Λ, as follows:

$$\Phi^T \mathbf{C}_v \Phi = \Lambda; \quad \mathbf{C}_v \Phi = \Phi \Lambda \tag{10}$$

Solution of the eigenvalue problem yields eigenvalues, $\Lambda = diag\{\lambda_1, \lambda_2, \ldots, \lambda_M\}$ (where $\lambda_1 > \lambda_2 > \ldots > \lambda_M$) and associated eigenvectors, $\Phi = \{\phi_1, \phi_2, \ldots, \phi_M\}$.

It is possible to rewrite the original M correlated time series, $\mathbf{V}(t)$, in terms of uncorrelated scalar subprocesses, $\mathbf{U}(t) = \{u_1(t), u_2(t), \ldots, u_M(t)\}^T$, such that

$$\mathbf{V}(t) = \Phi \mathbf{U}(t) = \sum_{j=1}^{M} \phi_j u_j(t) \tag{11}$$

where ϕ_j represents the j^{th} POD mode shape corresponding to the j^{th} scalar subprocess, $u_j(t)$. The energy associated with $u_j(t)$ is described in terms of the corresponding eigenvalue, λ_j. A reduced-order representation of the strain time series, $\hat{\mathbf{V}}(t)$, may be obtained by including only the first N POD modes and associated generalized coordinates:

$$\hat{\mathbf{V}}(t) = \sum_{j=1}^{N} \phi_j u_j(t), \qquad N < M \tag{12}$$

In the present study, strains are measured at twenty-three locations, i.e., $M = 23$. Following the procedure as outlined above, we can thus obtain twenty-three POD mode shapes, ϕ_j, and then decompose the original twenty-three strain time series into twenty-three uncorrelated POD scalar subprocesses, $u_j(t)$, which when scaled by the POD mode shapes reconstruct all the measurements in space and time.

Using the first thirteen POD modes which preserve 99% of the total field energy, the strain time series can be reconstructed at the location of the target sensor (strain sensor no. 4). Based on the first thirteen POD modes, the PSD for CF strain at each input logger and the summation of all these PSDs at each frequency are plotted in Figs. 5(a) and 5(b), respectively. Figure 5(c) shows that the reconstructed CF strain PSD (red dashed line) at the target sensor includes contributions from the first, third, and fifth harmonics, and matches the PSD based on measurements (blue solid line) reasonably well. In Fig. 5(d), RMS values of CF curvatures at the twenty-three input sensor locations based directly on measurements are indicated by the blue circles; at the location of the target sensor, the POD-based interpolation (indicated by the blue line which also shows estimated RMS values at other locations nearby) is very close to the RMS value (red cross) obtained from the measurements.

Recall that, POD modes are discrete along the spatial direction, i.e., the modal coordinates are only available at locations of the input sensors. If the location of interest (here it is the location of the target sensor) where no sensor is installed on, an interpolation of the POD-based modal coordinates between nearby sensors is needed. In this case, the target sensor lies between sensor nos. 3 and 5, and

Preprints (www.preprints.org) | NOT PEER-REVIEWED | Posted: 21 September 2018 doi:10.20944/preprints201809.0426.v1

the modal coordinates at the target may be interpolated quite effectively with a third-order polynomial fit using the decomposed POD-based modal coordinates at four nearby sensors (i.e., sensor nos. 2, 3, 5, and 6) mode by mode. Then the strain time series at the target location can be reconstructed using the interpolated modal coordinates based on Eq. 12. Similarly, the riser response at any location within the spread of the sensors, may be estimated by such piecewise interpolation and employing a subset of POD modes.

The fatigue damage ratio, representing the ratio of the estimated damage to that based directly on measurements, at the target sensor (i.e., sensor no. 4), is 1.05, which suggests that the fatigue damage is overestimated by 5% when the POD method is employed with thirteen POD modes. Similar results for other choices of the target sensor are discussed in Section 4.

Note that other interpolation techniques with different number of sensors may also be employed for interpolating the discrete POD modes. In addition to the third-order polynomial interpolation, the rational function interpolation [22] [23] and trigonometric/Fourier interpolations [24] were tested on simulated data sets as well as on NDP data sets. Results show that for the sensor arrangement of NDP data sets, the rational function interpolation often results in artificial poles, and the trigonometric function wiggles sharply sometimes, both cause huge errors in the interpolation; on the contrary, the third-order polynomial interpolation is easy to use, relatively stable, and almost always can provide reasonable results. Thus, in this study the third-order polynomial interpolation technique is selected to work with the POD method and another empirical method (Modal Phase Reconstruction) as seen in Section 3.4.

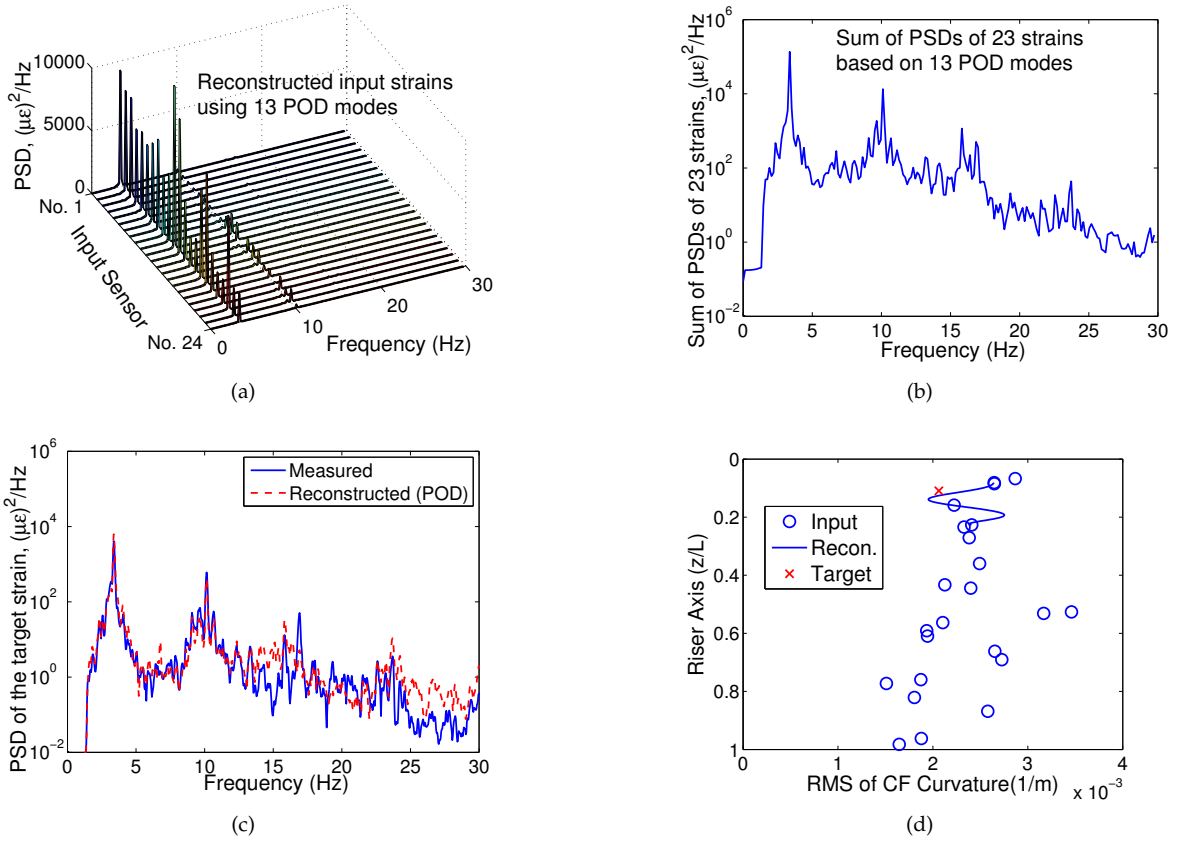

Figure 5: The POD procedure applied with twenty-three input sensors (sensor no. 4 is the target) for the NDP2350 (sheared current) data set: (a) PSDs of the strains at the twenty-three sensors reconstructed using the first thirteen POD modes; (b) Summation of the strain PSDs at each frequency using the first thirteen POD modes; (c) Strain PSD at the target sensor, reconstructed using thirteen POD modes vs. measured; and (d) RMS curvatures, reconstructed using thirteen POD modes vs. measured.

Preprints (www.preprints.org) | NOT PEER-REVIEWED | Posted: 21 September 2018 doi:10.20944/preprints201809.0426.v1

3.4. Modal Phase Reconstruction

As is the case with Proper Orthogonal Decomposition, the Modal Phase Reconstruction (MPR) method has the advantage in that mode shapes need not be assumed; they can be estimated empirically from the data. Lucor et al. [25] employed MPR to analyze riser response data from CFD simulations. Mukundan [19] applied MPR to the NDP data sets to analyze the influence of traveling waves on riser response. In this study, the MPR method is employed to analyze the NDP model riser response and to estimate fatigue damage at arbitrary locations along the length of the riser. The general framework for the MPR procedure is briefly presented here.

Assume that at location z_j, and at time instant, t_k, the riser response of interest (such as strain), i.e., $y(z_j, t_k)$, may be expressed as follows:

$$y(z_j, t_k) = Re\left\{\sum_{n=1}^{N} e^{i\omega_n t_k}\phi_n(z_j)\right\} \tag{13}$$

where $\omega_n = 2\pi n/(P\Delta t)$ is the n^{th} circular frequency; $t_k = k\Delta t$ is the k^{th} time sample; N is the number of frequency components included in the MPR procedure; P is the number of discrete time samples available in the record; and Δt is the sampling rate. Also, $Re\{\}$ represents the real part of the associated (complex) function. Note that $\phi_n(z_j)$ is the n^{th} complex mode coordinate—with real part, $\phi_{n,Re}(z_j)$, and imaginary part, $\phi_{n,Im}(z_j)$—at location, z_j, which needs to be empirically estimated from the data.

Equation 13 may be written in compact form as follows:

$$y(z_j, t_k) = Re\left\{\Delta_k \Phi_j\right\} \tag{14}$$

where $\Delta_k = \left[e^{i\omega_1 t_k}, e^{i\omega_2 t_k}, \ldots, e^{i\omega_N t_k}\right]$, and $\Phi_j = \left[\phi_1(z_j), \phi_2(z_j), \ldots, \phi_N(z_j)\right]^T$.

Then at location, z_j, the riser response recorded at all P discrete time instants may be expressed as follows:

$$y(z_j) = Re\left\{\hat{\Delta}\Phi_j\right\} \tag{15}$$

where $y(z_j) = \left[y(z_j, t_1), y(z_j, t_2), \ldots y(z_j, t_P)\right]^T$ represents the entire recorded response time series at location, z_j; and $\hat{\Delta} = [\Delta_1, \Delta_2, \ldots, \Delta_P]^T$ is easily defined given information only on the length and the sampling rate of the record. In Eq. 15, it is mode shape matrix, Φ_j, that needs to be estimated; the MPR method, thus, defines this system of P equations and $2N$ unknowns (since each $\phi_n(z_j)$ contained in Φ_j has real and imaginary parts). As long as $2N \leq P$, this system of equations can be used to solve for Φ_j in a least squares sense.

As is the case with the POD method, the MPR method only yields empirically estimated mode shape coordinates at those discrete locations where the riser response is measured. If the riser response is to be estimated at a location where no sensor is present, it is necessary to interpolate the real and imaginary parts of the N mode shapes to the desired location and to, then, reconstruct the response there by accounting for all these N modes or frequency components. Equation 13, used for the reconstruction, may be rewritten as follows:

$$y(z_j, t_k) = \sum_{n=1}^{N}\left[\phi_{n,Re}(z_j)\cos(\omega_n t_k) - \phi_{n,Im}(z_j)\sin(\omega_n t_k)\right] \tag{16}$$

To speed up the computation, the measured riser strains are downsampled by a factor of 5, effectively reducing the data sampling frequency from 1,200 Hz to 240 Hz, which shrinks the number of time samples, P, in each record, to one-fifth of its original value. Additionally, instead of decomposing the measurements so as to represent all the complex modes or frequency components (from 0 Hz to the Nyquist frequency, $N = P/2$), the number of modes, N, is selected such that the frequency band from ω_1 to ω_N preserves 99% of the total energy (defined as the sum of the variance of the strains at all the

Preprints (www.preprints.org) | NOT PEER-REVIEWED | Posted: 21 September 2018 doi:10.20944/preprints201809.0426.v1

loggers). Figure 6(a) shows CF PSDs for all the input sensors (except sensor no. 4). In Fig. 6(b), the sum of PSDs of the twenty-three input CF strains (excluding the strain at the target sensor, i.e., logger no. 4) is represented by the blue line; the selected frequency band that preserves 99% of the total energy is indicated by the red dots. By decomposing the riser strain measurements into modes only over the 99%-energy frequency band, the number of frequency components, N, is reduced to one-seventh of its original value. This greatly reduces the number of coefficients to be determined in the MPR linear system solution and, hence, dramatically saves computational time. Figure 6(c) shows that the energy distribution by frequency of the reconstructed CF strains at the target sensor (red dashed line) matches that based on the measured strains there (blue solid line) reasonably well over the 99%-energy frequency band. In Fig. 6(d), RMS values of CF curvatures at the twenty-three input sensor locations based directly on measurements are indicated by the blue circles; at the location of the target sensor, the MPR-based interpolation (indicated by the blue line which also shows estimated RMS values at other locations nearby) is very close to the RMS value (red cross) obtained from the measurements. The strains at the target sensor (no. 4) are interpolated quite effectively with a third-order polynomial fit using strains from four nearby sensors, i.e., sensor nos. 2, 3, 5, and 6 (again, other fits are also possible). As is the case with the POD procedure, riser response statistics, such as the RMS CF curvature, at any location within the spread of the sensors, may be estimated by such piece-wise interpolation following application of the MPR procedure.

The fatigue damage ratio, representing the ratio of the estimated damage to that based directly on measurements, at the target sensor (i.e., sensor no. 4), is 1.25, which suggests that the fatigue damage is overestimated by 25% when the MPR method is employed with the selected frequency components. Similar results for other choices of the target sensor are discussed in Section 4.

3.5. Hybrid Method: MPR + Modified WWA

By studying Eq. 16, it may be noted that the MPR method decomposes the measured riser response into N components and, importantly, each component is a single-frequency time series. This suggests that the each single-frequency component may be decomposed further by using the previously discussed modified WWA method. This approach is referred to as the "hybrid" method since it combines the MPR and the modified WWA methods. The hybrid method has two advantages when compared with either the MPR or the modified WWA methods. First, unlike the MPR method, the hybrid method does not require interpolation from discrete complex modes to estimate or reconstruct the response at any arbitrary location; it has the ability to reconstruct the riser response over the entire length of the riser (as a continuous function) despite starting from only a discrete number of measurements. Second, the modified WWA method seeks to represent several frequency components of a wide-band (multi-frequency) response time series with the help of measurements from available sensors; on the other hand, the hybrid method seeks to decompose each MPR mode for a single frequency defined at the same sensors.

Application of the hybrid method procedure is presented below. First, the MPR approach is followed and the various input strains are represented as in Eq. 16. Then, at the location of each input sensor, z_j, the real part of the n^{th} MPR mode, $\phi_{n,Re}(z_j)$, may be decomposed using the modified WWA procedure as follows:

$$\phi_{n,Re}(z_j) = \sum_{k=1}^{s} \left[a_k \varphi_k(z_j) + b_k \psi_k(z_j) \right] \tag{17}$$

where $\varphi_k(z_j)$ and $\psi_k(z_j)$ are defined in exactly the same manner as in Eq. 9. The real part of the n^{th} MPR mode at locations of all M sensors may be expressed in matrix form (as in Eq. 6), i.e., $\mathbf{Aw} = \mathbf{d}$, where $A_{j,2i-1} = \varphi_i(z_j)$ and $A_{j,2i} = \psi_i(z_j)$, and $d_j = \phi_{n,Re}(z_j)$. As long as $2s \leq M$, the modal weights, ($\mathbf{w}^T = \{a_1, b_1, a_2, b_2 \ldots a_s, b_s\}$), may be estimated in a least-squares sense, and a spatially continuous function, $\phi_{n,Re}(z)$, can be derived. Note that exactly the same procedure may be repeated to decompose the imaginary part of the n^{th} MPR mode, i.e., for $\phi_{n,Im}$. By iterating this procedure for all the real and

Preprints (www.preprints.org) | NOT PEER-REVIEWED | Posted: 21 September 2018 doi:10.20944/preprints201809.0426.v1

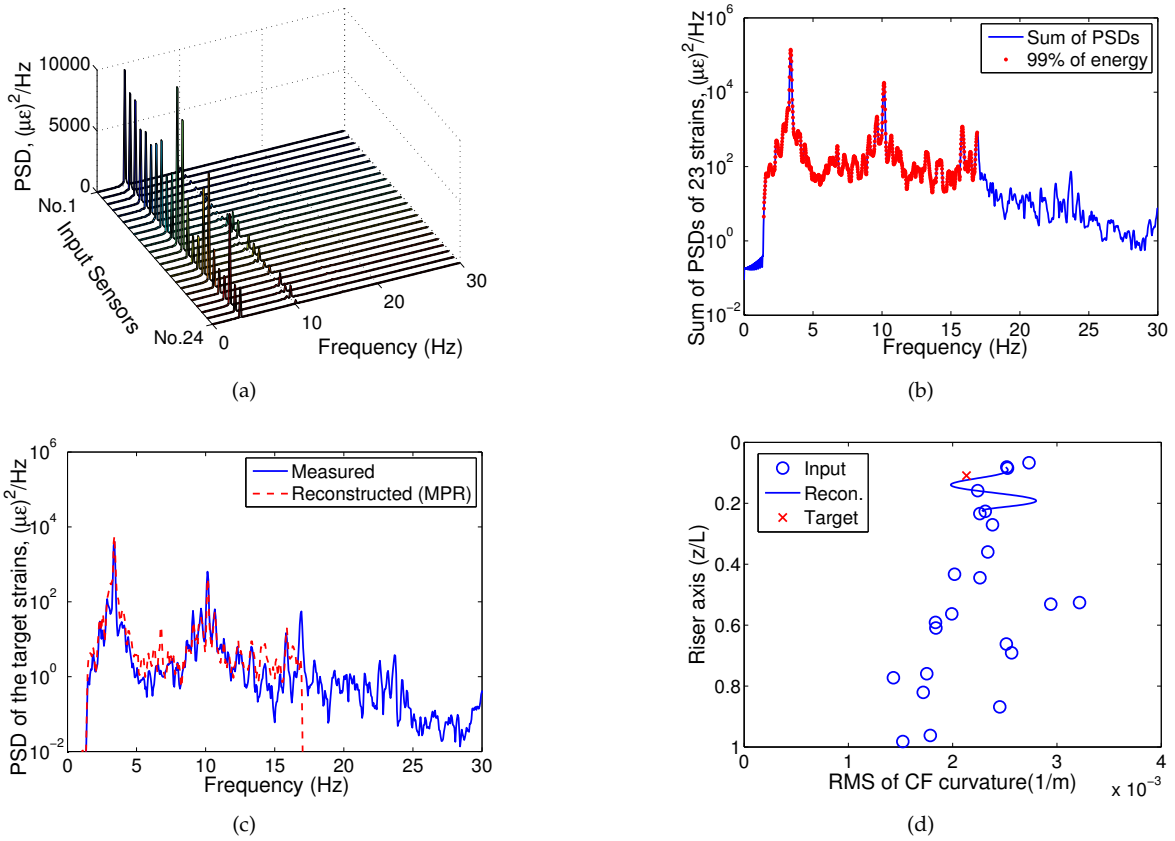

Figure 6: The MPR procedure applied with twenty-three input sensors (sensor no. 4 is the target) for the NDP2350 (sheared current) data set: (a) PSDs of the strains measured at the twenty-three sensors; (b) Summation of the strain PSDs and the frequency components that preserve 99% energy; (c) Strain PSD at the target sensor, reconstructed (using modes that preserve 99% energy) vs. measured; and (d) RMS curvatures, reconstructed (using modes that preserve 99% energy) vs. measured.

imaginary MPR modes, the riser response over its entire span can be reconstructed as a continuous function by this hybrid method. In the present study, where $M = 23$, we use s equal to 6; the modes in the modified WWA portion of the hybrid method are selected to correspond to frequencies closest to the MPR mode that is being reconstructed according to Eq. 17.

An example using the hybrid method with strain sensor no. 4 as the target sensor is presented in Fig. 7, which may be compared directly with Fig. 6 based on the MPR procedure.

The fatigue damage ratio, representing the ratio of the estimated damage to that based directly on measurements, at the target sensor (i.e., sensor no. 4), is 1.84, which suggests that the fatigue damage is overestimated by 84% when the hybrid (MPR-modified WWA) method is employed with the selected frequency components. Similar results for other choices of the target sensor are discussed in Section 4.

4. FATIGUE DAMAGE ESTIMATION BASED ON A LARGE NUMBER OF SENSORS

The CF strains on the NDP model riser were measured using twenty-four strain sensors (only twenty-three sensors were available for the NDP2420 data set, since strain sensor no. 21 had failed). In the results described here, we select one sensor at a time as the target sensor, and use measurements from the remaining twenty-three (or twenty-two) sensors to reconstruct strains at the location of the target sensor by employing the various empirical methods described above. Such analysis for each empirical method applied with sensor no. 4 as the target sensor is presented in the previous section (Section 3). The damage ratio, which represents the ratio of the fatigue damage rate based on the

Preprints (www.preprints.org) | NOT PEER-REVIEWED | Posted: 21 September 2018 doi:10.20944/preprints201809.0426.v1

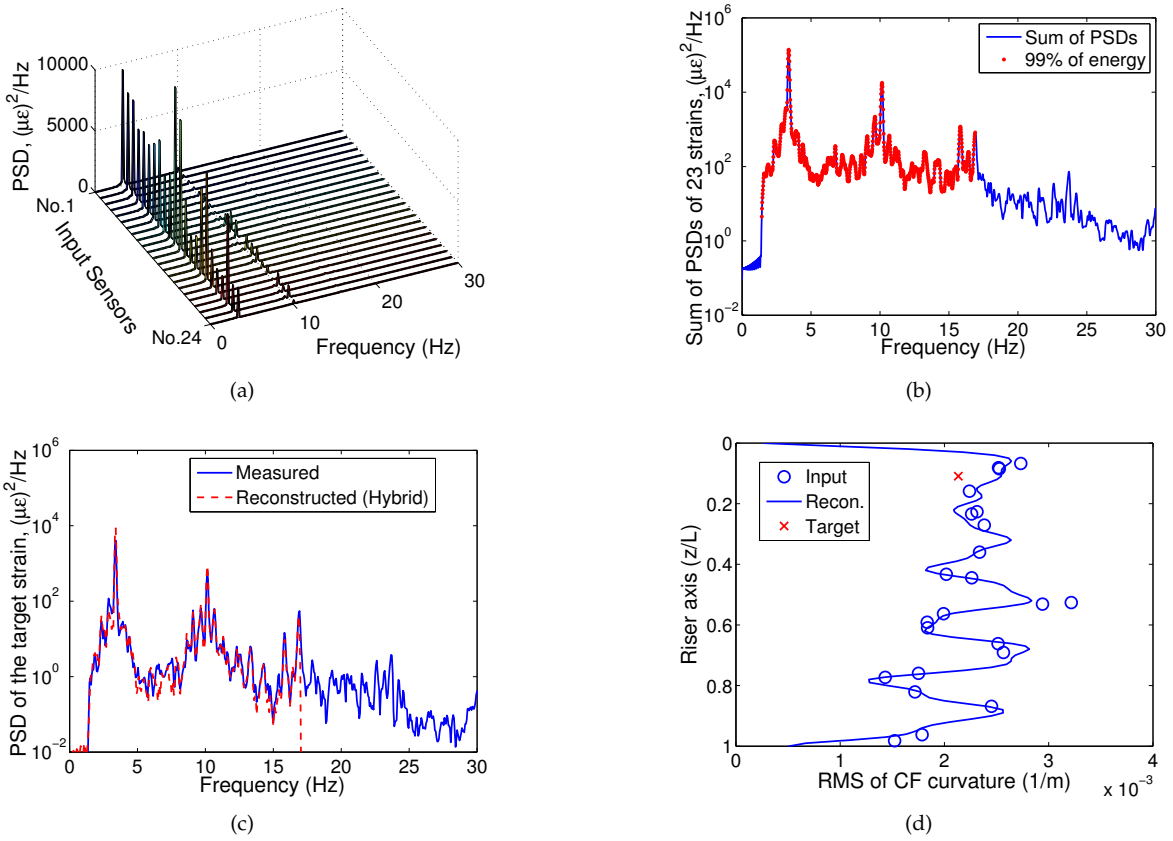

Figure 7: The hybrid (MPR + modified WWA) procedure applied with twenty-three input sensors (sensor no. 4 is the target) for the NDP2350 (sheared current) data set: (a) PSDs of the strains measured at the twenty-three sensors; (b) Summation of the strain PSDs and the frequency components that preserve 99% energy; (c) Strain PSD at the target sensor, reconstructed (using modes that preserve 99% energy) versus measured; and (d) RMS curvatures, reconstructed (using modes that preserve 99% energy) vs. measured.

reconstructed strain (at the target sensor) to that based directly on the measured strain there, is used as a criterion to compare the empirical methods. Figure 8 presents damage ratios estimated at the twenty-four locations for the two uniform current data sets (red color) and the two sheared current data sets (blue color), by employing each of the five empirical methods. The lowest and highest values of the damage ratios estimated on each data set using each empirical method, are also indicated in the figure legends—for example, Fig. 8(a) states that the twenty-four damage ratios estimated by the WWA method on the NDP2120 uniform current data set ranged from 0.25 to 6.58.

Some general conclusions, that may be drawn by studying Fig. 8, are summarized here.

(i) With the WWA method, a large number of modes can be interpreted from a suite of measurements. The modified WWA method can better account for the effects of traveling waves and localized curvature changes but fewer modes can be interpreted or used in reconstruction of strains at any target location. As a consequence, in this study where a large number of sensors (twenty-three) are available, fatigue damage rates estimated over the entire riser length by the WWA and the modified WWA methods are generally of comparable accuracy (see Figs. 8(a) and 8(b)).

(ii) Fatigue damage rates estimated by the POD and MPR methods are quite similar since both methods are affected by the quality of the unavoidable interpolation—it may be noted that the presence of sensors close to the target location leads to a good estimation of the fatigue damage; however, when nearby sensors are not present, as is the case for sensor no. 9 indicated by the red ellipses in Figs. 8(c) and 8(d), fatigue damage estimates are less accurate.

 doi:10.20944/preprints201809.0426.v1

(iii) The fatigue damage rates of the two uniform current data sets estimated either by the POD or the MPR methods are less accurate than those estimated by the WWA or the modified WWA methods; one likely reason for this is due to the strong non-stationary response characteristics indicated particularly in the two uniform current data sets (see Shi et al. [26]) that more directly affect the accuracy of the POD and the MPR methods. With the WWA and the modified WWA methods, the modal weights are solved for at each time instant (see Eq. 7); the POD and the MPR methods, on the other hand, assume that the riser response is described by a stationary process and decomposition of the measured response is based on the entire record (see Eqs. 10 and 15). To reduce the influence of the non-stationarity of the measured response on fatigue damage estimations, one possible approach is to divide the recorded response time series into shorter segments and then to employ the POD or MPR methods on shorter segments.

(iv) Generally, when a large number of sensors available, as is the case with the NDP model riser, all the five empirical methods estimate fatigue damage rates over the entire riser length quite well: damage ratios are typically in the range from 0.3 to 3.0, with the lowest and highest estimations of 0.16 and 14.54, respectively. Among the five methods, the hybrid method (Fig. 8(e)) which combines the MPR and the modified WWA procedures, is the most accurate for fatigue damage estimation.

In Section 3 it is stated that the damage ratio is more critical to the error of the reconstructed rise response than the strain-RMS ratio or the displacement-RMS ratio. This is the reason of choosing the damage ratio as the scalar to evaluate different empirical methods. In order to illustrate this point, the ratio of the fatigue damage rates, the ratio of RMS values of strain, and the ratio of RMS values of displacement are calculated using WWA procedure with 23 input sensors for the NDP2350 data set. Figure 9 shows that the damage ratio falls in the range of 0.36 to 14.54, while the strain-RMS ratio falls in the range of 0.60 to 2.24 and the displacement-RMS ratio falls in the range of 0.34 to 2.14. The damage ratio has the widest range (i.e., most critical to errors) and, thus, serves best as an indicator of the accuracy of the reconstructed riser response.

In addition to the NDP data sets, two sets of synthetic riser motion data are simulated for the evaluation of the empirical response reconstruction methods. One set contain three standing waves of different frequencies, amplitudes and wavelengths; another set contain one standing wave and two traveling waves. The riser physical properties and sensor arrangement are identical to the NDP model riser. Using measurements at sensor locations with each empirical method, the riser response is reconstructed and, then, compared with the true/simulated response over its entire span. Similar observations as on the NDP data sets were obtained on the simulated data sets. Generally, given enough number of sensors, the five empirical methods all can be employed to reconstruct the riser responses and, then, to estimate the fatigue damages quite well, despite different underlying assumptions and advantages/disadvantages in each of them.

5. FATIGUE DAMAGE ESTIMATION BASED ON A SMALL NUMBER OF SENSORS

The estimation of fatigue damage rates over the entire length of the NDP model riser based on measurements from a large number of sensors was discussed in the previous section (Section 4). However, actual deepwater drilling risers are seldom instrumented as densely as the NDP model riser, due to the high cost of sensor deployment, maintenance, data retrieval, etc. Accordingly, it is desired to discuss estimation of fatigue damage rates over the riser length based on measurements from a much smaller number of sensors than before. Using strain measurements from eight sensors as inputs, the riser response is reconstructed at the locations of all of the twenty-four sensors (including the eight input sensors). By iterating over numerous different combinations of eight strain sensors as inputs (from among all the twenty-four available sensors on the riser), optimal locations for the eight sensors along the riser are identified by cross-validation, whereby estimated strains and fatigue damage rates at the twenty-four locations are compared with strains and fatigue damage rates based on the actual recorded measurements there.

Preprints (www.preprints.org) | NOT PEER-REVIEWED | Posted: 21 September 2018 doi:10.20944/preprints201809.0426.v1

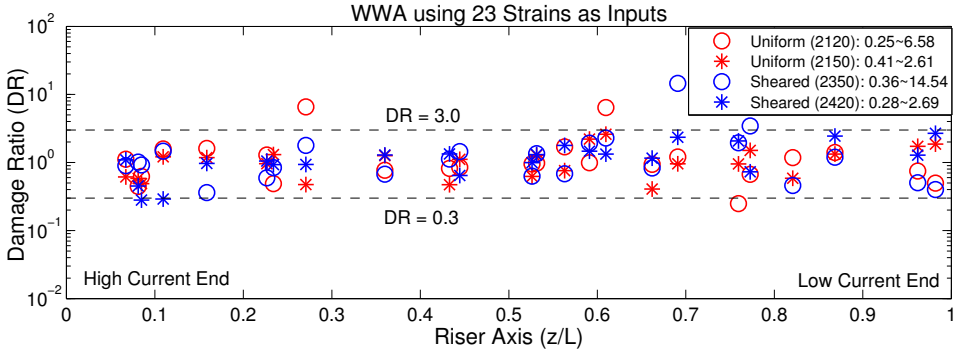

(a)

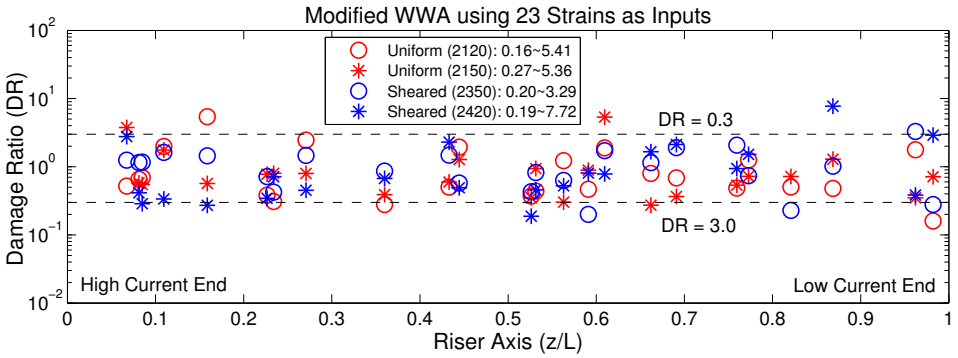

(b)

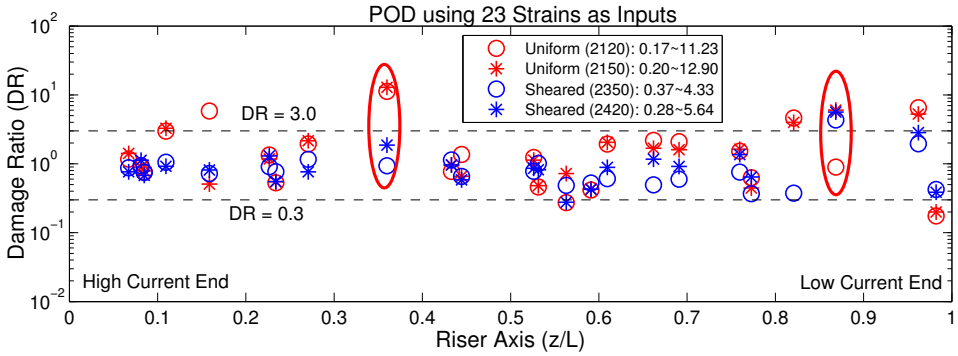

(c)

Figure 8. Fatigue damage ratios estimated by different empirical methods at all locations along the NDP model riser, using twenty-three stains as inputs: (a) WWA; (b) Modified WWA; (c) POD; (d) MPR; and (e) Hybrid: MPR + modified WWA.

In principle, all the possible combinations of eight sensors chosen from twenty-four available could be selected; however, this results in an exceedingly large number of combinations to be evaluated. Thus, only thirty-four arrangements or combinations of eight sensors are selected for the fatigue damage analysis. Figure 10 shows the locations of the eight sensors for the thirty-four selected combinations. The first group (identified as G1) comprises sixteen combinations, each of which includes eight contiguous sensors; the second group (G2) has six combinations wherein six sensors are located near the top end (i.e., the higher current end in the case of the sheared current data sets) and the remaining two sensors are near the middle, at a location around one-fourth of the riser's length

Preprints (www.preprints.org) | NOT PEER-REVIEWED | Posted: 21 September 2018 doi:10.20944/preprints201809.0426.v1

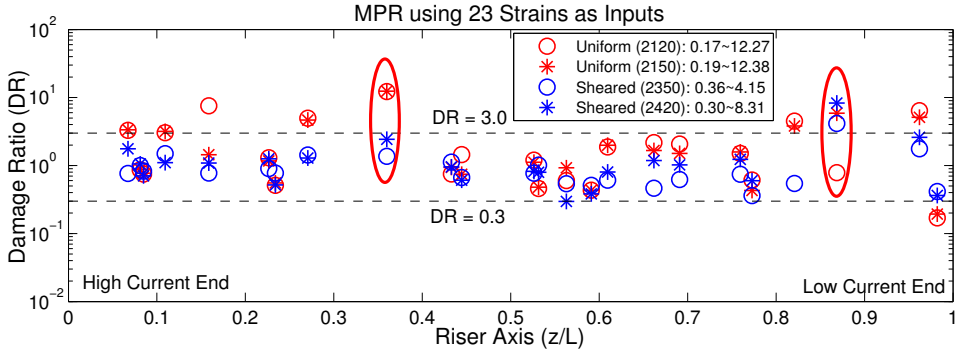

(d)

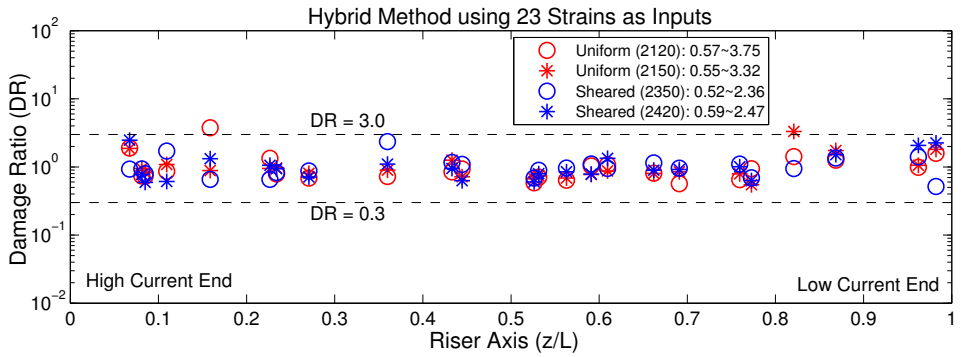

(e)

Figure 8. Fatigue damage ratios estimated by different empirical methods at all locations along the NDP model riser, using twenty-three stains as inputs (cont.): (a) WWA; (b) Modified WWA; (c) POD; (d) MPR; and (e) Hybrid: MPR + modified WWA.

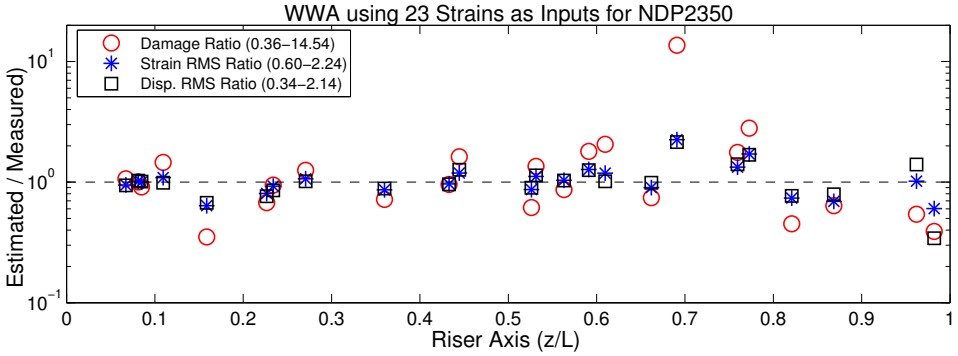

Figure 9: Scalars might be used to evaluate the reconstructed riser response, including damage ratio, strain RMS ratio, and displacement RMS ratio.

from the bottom (low current) end, or at the bottom end. Note that a malfunctioning strain sensor (no. 21) is not selected as an input sensor in these studies.

Note that not all the five empirical methods discussed earlier are employed here that uses eight strain sensors to estimate fatigue damage; there are reasons for this. First, for the modified WWA method, only two or three modes could be represented if eight sensors are available; this would make it difficult to account for all the important frequencies (the first and higher harmonics) of the riser responses. Second, for the POD and MPR methods, the accuracy of the interpolation (from

Preprints (www.preprints.org) | NOT PEER-REVIEWED | Posted: 21 September 2018 doi:10.20944/preprints201809.0426.v1

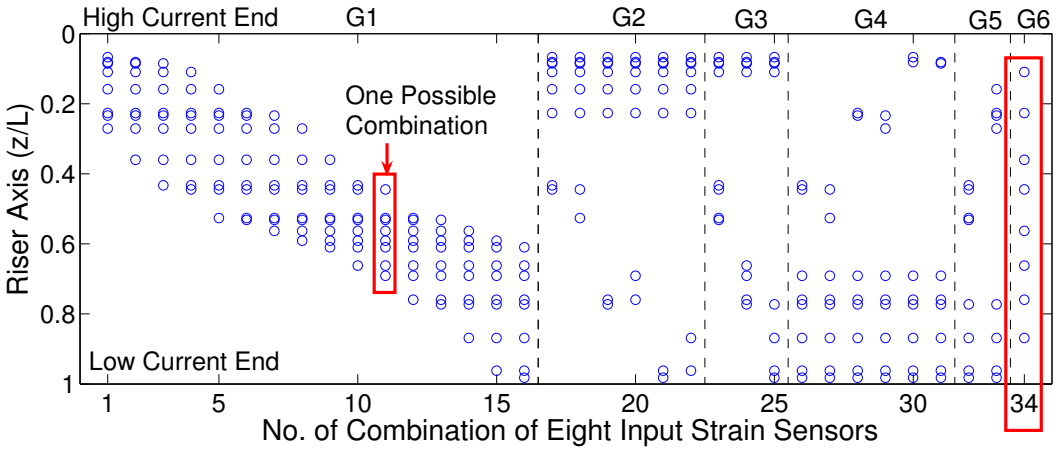

Figure 10: Thirty-four combinations of eight input strain sensors chosen for fatigue damage analysis studies using cross-validation against measurements.

information at the discrete locations of the input sensors to all other locations) controls the accuracy of the reconstructed riser response at target locations without sensors. If the target location has no available sensors nearby or if it is spatially outside the range of the suite of input sensors, the reconstructed riser response will be inaccurate. Given these limitations, the modified WWA, POD and MPR methods are not employed in this study with eight input sensors; only the WWA and the hybrid methods are employed to estimate fatigue damage rates at the twenty-four locations along the NDP model riser using measurements from eight sensors.

The base-10 logarithms of the 24 damage ratios (DRs) estimates from the WWA method based on eight sensors in each of the thirty-four combinations are presented as box-and-whisker plots in Figs. 11(a) and 11(b), which summarize results for the two uniform current data sets and the two sheared current data sets, respectively. In each box-and-whisker plot, the central mark and the edges of the box represent the median, the 25th percentile, and the 75th percentile of the data; the upper and lower whiskers extend out to the minimum and the maximum values. A shorter bar indicates low variability or greater precision in the estimation of the damage ratios; vertically, the closer the bar is to unity, the more accurate is the estimation. Preferred combinations that ensure precise and accurate estimation of the fatigue damage rate for all the four data sets are indicated by green arrows. When employing the WWA method, the use of eight sensors distributed over a greater portion of the riser, e.g., placing four sensors near one end and four sensors near the other end, such as in combinations nos. 25 or 33, generally results in more accurate and precise fatigue damage estimation than does the use of eight clustered sensors such as in combination nos. 1 to 16.

Fatigue damage ratios estimated by the hybrid method based on eight sensors (using four modes) in each of the thirty-four combinations are illustrated by box-and-whisker plots in Figs. 12(a) and 12(b) which summarize results for the two uniform current data sets and the two sheared current data sets, respectively. Direct comparison with the results based on the WWA method (see Fig. 11) suggest that among the thirty-four combinations, those that were identified as more precise and accurate based on results with the WWA method were also found to be so with the hybrid method. For all the thirty-four combinations, the hybrid method was found to generally provide more accurate and precise estimations of the fatigue damage rates than the WWA method does.

6. SENSOR LOCATION AND SPATIAL ALIASING

Efficient sensor location and possible spatial aliasing errors for risers are conveniently studied by examining the $N \times N$ orthogonality matrix, $\mathbf{R}$, defined in terms of N modes of interest [9]—i.e., $\mathbf{R}_{i,j} = |\varphi_i^T \varphi_j|$ $(i, j = 1, \ldots, N)$ where, for example, if sinusoidal mode shapes are assumed, $\varphi_i =$

Preprints (www.preprints.org) | NOT PEER-REVIEWED | Posted: 21 September 2018 doi:10.20944/preprints201809.0426.v1

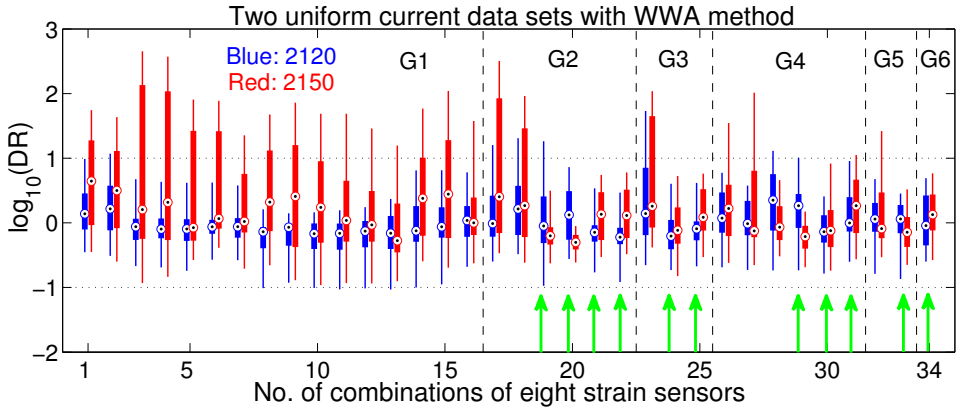

(a)

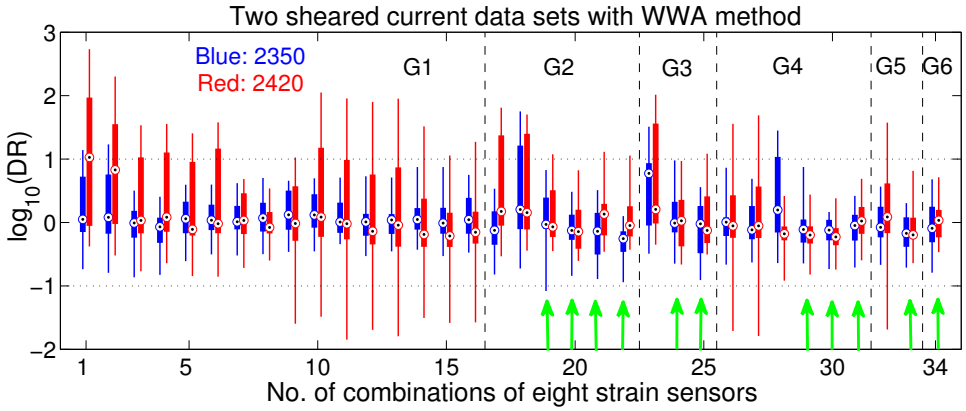

(b)

Figure 11: Fatigue damage ratios estimated by the WWA method from measurements based on thirty-four combinations involving eight strain sensors: (a) Two uniform current data sets; and (b) Two sheared current data sets.

$[sin(n_i\pi z_1/L), sin(n_i\pi z_2/L), \ldots sin(n_i\pi z_M/L)]$ when M loggers are employed on a riser of length, L. For an array of sensors that avoids aliasing errors, off-diagonal terms of **R** are relatively small (the diagonal terms are less important but are generally close to unity). Figure 13(a) shows off-diagonal terms of the orthogonality matrix computed for the twelve modes used with the WWA method with twenty-three sensors (sensor no. 4 is the target) for the NDP2350 sheared current data set. Figure 13(b) is a similar plot where eight sensors (associated with combination no. 34) are used and six modes were employed with the WWA method. The relatively low values of the off-diagonal elements of **R** in the figures confirms that spatial aliasing is not of great concern in the choice of sensor locations in the WWA and modified WWA method results presented. Note that the orthogonality matrix, **R**, for the modified WWA method can be constructed in a similar manner as for the WWA method.

Spatial distribution of the loggers may also, in general, be of concern when the MPR and POD methods are employed. This is not so much a spatial aliasing issue; rather, these two methods rely on interpolation from discrete sensor locations (from relevant POD or MPR modes) to any target location while reconstructing strains there. If the target location is spaced very far from the closest sensors used in the interpolation, reconstructed strains can be quite inaccurate. Even if higher modes are well represented in the POD or MPR modes derived, because these modes are discrete, poor interpolation might lead to spurious understanding of the higher harmonics at the target location since these are associated with smaller wave lengths, which will accentuate problems due to interpolation when sensor distribution is not dense.

Preprints (www.preprints.org) | NOT PEER-REVIEWED | Posted: 21 September 2018 doi:10.20944/preprints201809.0426.v1

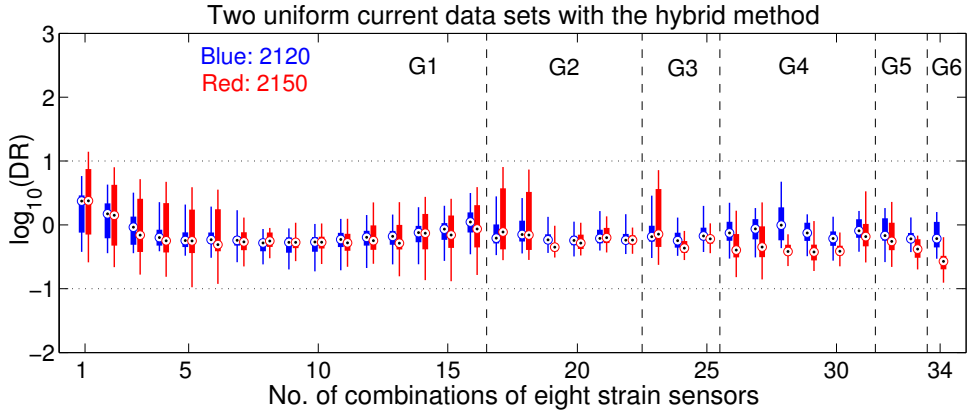

(a)

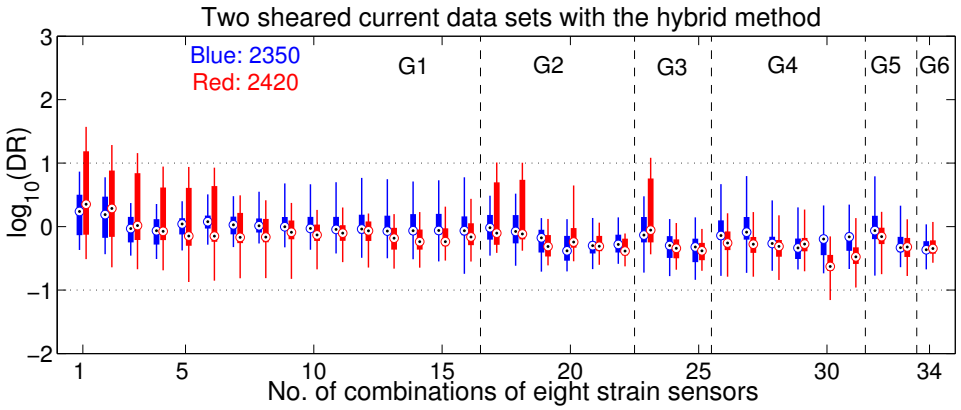

(b)

Figure 12: Fatigue damage ratios estimated by the hybrid method based on thirty-four combinations involving eight strain sensors: (a) Two uniform current data sets; and (b) Two sheared current data sets.

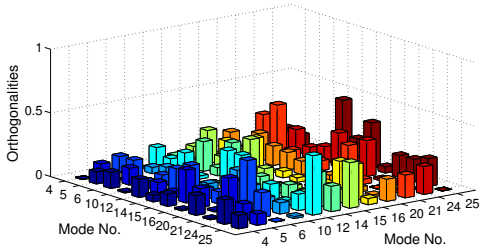

(a)

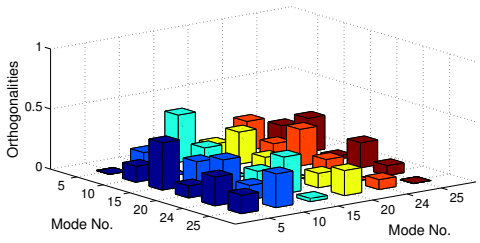

(b)

Figure 13: Off-diagonal elements of orthogonality matrices, **R**, computed with assumed sinusoidal mode shapes for the NDP2350 (sheared current) data set: (a) Twenty-three sensors and twelve WWA modes used (sensor no. 4 is the target); and (b) Eight sensors and four WWA modes (combination no. 34).

7. DISCUSSIONS

In this study, four data sets comprising strains measured on the NDP model riser subjected to uniform and sheared currents were employed to test empirical fatigue damage estimation methods. Five empirical methods were studied—they include Weighted Waveform Analysis (WWA), modified WWA, Proper Orthogonal Decomposition (POD), Modal Phase Decomposition (MPR), and a hybrid

 doi:10.20944/preprints201809.0426.v1

method that combines MPR and modified WWA. For each method, the theoretical formulation was first presented briefly and then its application was illustrated by an example wherein a single sensor was selected as the target sensor and by using measurements from the remaining twenty-three sensors as inputs, the riser response was reconstructed at the location of the target sensor. The fatigue damage rate estimated using the reconstructed riser response was compared with the value based directly on the measurements at that target. The ratio between the estimated fatigue damage and that based on measurements there was used as an indicator of the accuracy of the empirical method. Two separate summary studies—one involving a larger number of available sensors on the riser (twenty-three) and another involving a small number (eight)—were carried out and estimated fatigue damage rates over the entire length of the NDP model riser were computed and the results discussed.

Based on the numerical studies presented, some concluding remarks follow:

(i) With careful selection of the riser modes for inclusion, the WWA method has the ability to preserve higher harmonics in the reconstructed riser response since the selected modes in the method are non-sequential. Because the modal weights are solved for at each time instant, non-stationary characteristics, if present, have limited influence on response reconstruction with this method. The WWA method works particularly well if only a small number of sensors is available and relies on assumed mode shapes that are based on knowledge of the physical properties of the riser. Computation with the WWA method is fast.

(ii) The modified WWA method can account for the influence of higher harmonics as long as a large number of sensors is available. This method is more versatile in accounting for the effect of traveling waves than the WWA method. Like the WWA method, it also accounts for non-stationary characteristics, but it is not well-suited for cases where only a small number of sensors is available since a greater number of modal weights need to be estimated than with WWA. The modified WWA method relies on assumed mode shapes and computation is fast.

(iii) The POD method preserves frequency components and higher harmonics in the reconstructed riser response by empirical decomposition of the spatio-temporal data. This is evident from the power spectra as well as curvature plots that reveal high-frequency energy and large curvatures (or small wavelengths), respectively. POD only relies on data; the method identifies empirical mode shapes directly from data, without the need for physical properties of the riser. The POD scheme is the fastest among the five methods; however, POD does not account for non-stationary response characteristics. The method is not well-suited when only a small number of sensors is available because of inaccuracies in the reconstructed response that arise due to the need for interpolation or extrapolation.

(iv) As is the case for the POD method, the MPR method accounts for higher harmonics in the response and only relies on data, not on physical properties of the riser to estimate complex riser modes. MPR, however, is not well-suited to situations where the riser response exhibits strong non-stationary characteristics or when only a small number of sensors is available. Computation with the MPR method is slow. Importantly, MPR explicitly accounts for traveling waves in decomposing the measured response.

(v) The hybrid method (which combines the MPR and modified WWA methods) has the ability to account for higher harmonics and the effect of traveling waves; it also works quite well even if only a small number of sensors is available. The hybrid method does not explicitly take into consideration non-stationary characteristics, but reconstruction even with fairly strong non-stationary response is superior to that with the POD and MPR methods. The hybrid method needs to assume modes in the second step of estimating modal weights for the complex MPR modes. Although the hybrid method is the slowest due to the greater computational effort relative to the other methods, it is the most accurate both for a large as well as a small number of input sensors.

There are some limitations of this study that need to be addressed at this point. First, the results are based on four NDP data sets and two simulated data sets only. The uncertainty or confidence bounds on fatigue damage estimates from each empirical method is not directly discussed. Second, the issues, that relate to what constitutes an adequate sample in terms of length of the measured signal and

 doi:10.20944/preprints201809.0426.v1

sampling rate when employing each empirical method for reconstruction of strain and fatigue damage estimation, are not directly addressed. Third, in this study, only strain measurements are employed in the fatigue damage estimation. However, it should be noted that acceleration measurements or a combination of strain and acceleration measurements may also be employed to estimate fatigue damage.

8. CONCLUSIONS

There are many factors may affect the accuracy of the response reconstruction and the selection of method, such as the pattern of waves (standing or traveling waves), the arrangement of sensors (number and spacing), the nonstationary characteristics of riser response, complex configuration of risers (distribution of mass and buoyancy), and unknown boundary conditions, etc. It is impossible to examine all the factors in the current work. Based on the studies using the available NDP data sets and the simulated data (results of using simulated data are not included in this paper), some conclusions may be summarized as:

(i) For the case where traveling waves are not dominated in the riser's response, WWA is preferred over the modified WWA to provide the response reconstruction over the entire riser span. For the case where strong traveling waves exist and enough number of sensors are available, the modified WWA may be a better choice than WWA procedures.

(ii) If none or few physical information of risers is available, POD or MPR may be employed to estimate the riser's response over the region where sensors are closely spaced, no matter whether traveling wavers exist or not.

(iii) The hybrid method seems to be the most accurate among the five methods tested, no matter how prevalent the traveling waves are and how many sensors are available. However, due to a limited number of data set tested, this conclusion is tentative, and the method should be applied with caution.

Note that these empirical methods are always not perfect. Riser responses reconstructed by these methods are encouraged to be checked against the understanding of the riser behavior based on engineering judgement. Furthermore, the uncertainties/errors of the estimated fatigue damage rate can be quantified through a cross-validation analysis which is incorporated with such empirical procedures. After "short-term" fatigue damage distributions conditional on specific current profiles are obtained using such empirical methods, it is possible next to estimate the "long-term" fatigue life of risers by integrating the short-term fatigue damage distributions (corrected by the uncertainties factors) with the likelihood of different current profiles. As the result, the long-term fatigue damage and the fatigue failure probability may be estimated using the empirical methods with riser response measurements [27].

Author Contributions: methodology, validation, and original draft preparation, Chen Shi; review, editing and supervision, Lance manuel; funding acquisition, Michael Tognarelli.

Funding: Financial supports by National Key R&D Program "Research, development and project demonstration of a multipurpose flexible pipe for ultra-deepwaters (Grant No. 2016YFC0303800)", Fundamental Research Funds for Central University (Grant No. 16CX02024A), and BP America Production Co. are greatly appreciated.

Acknowledgments: The authors acknowledge with gratitude the permission granted by the Norwegian Deepwater Programme (NDP) Riser and Mooring Project to use the Riser High Mode VIV test data.

Conflicts of Interest: The authors declare no conflict of interest. The founding sponsors had no role in the design of the study; in the collection, analyses, or interpretation of data; in the writing of the manuscript, or in the decision to publish the results.

Abbreviations

The following abbreviations are used in this manuscript:

VIV	Vortex-induced vibration
WWA	Weighted waveform analysis
POD	Proper orthogonal decomposition
MPR	Modal phase reconstruction
CF	Cross-flow
IL	Inline
RMS	root-mean-square

References

1. Tognarelli, M.A. and Taggart, S. and Campbell, M. Actural VIV Fatigue Response of Full Scale Drilling Risers: with and without Suppression Devices. *27th International Conference on Offshore Mechanics and Arctic Engineering* **2008**, *Paper no. 57046*, Estoril, Portugal.
2. Vandiver, J.K. and Swithenbank, S.B. and Jaiswal, V. and Jhingran, V. Fatigue Damage from High Mode Number Vortex-Induced Vibration. *25th International Conference on Offshore Mechanics and Arctic Engineering* **2006**, *Paper no. 9240*, Hamburg, Germany.
3. Jhingran, V. and Vandiver, J.K. Incorporating the Higher Harmonics in VIV Fatigue Predictions. *26th International Conference on Offshore Mechanics and Arctic Engineering* **2007**, *Paper no. 29352*, San Diego, USA.
4. Modarres-Sadeghi, Y. and Mukundan, H. and Dahl, J.M. and Hover, F.S. and Triantafyllou, M.S. The Effect of Higher Harmonic Forces on Fatigue Life of Marine Risers. *Journal of Sound and Vibration* **2010**, *329*, 43-55.
5. Meneghini, J.R. and Saltara, F. and Fregonesi, R.A. and Yamamoto, C.T. and Casaprima, E. and Ferrari, J.A. Numerical simulations of VIV on long flexible cylinders immersed in complex flow fields. *European Journal of Mechanics B/Fluids* **2004**, *23* , 51-63.
6. Yamamoto, C.T. and Meneghini, J.R. and Saltara, F. and Fregonesi, R.A. and Ferrari, J.A. Numerical simulations of vortex-induced vibration on long flexible cylinders. *Journal of Fluids and Structures* **2004**, *19*, 467-489.
7. Huang, K. and Chen, H.C. and Chen, C.R. Vertical riser VIV simulation in uniform current. *Journal of Offshore Mechanics and Arctic Engineering* **2010**, *132*, 1-10.
8. Trim, A.D. and Braaten, H. and Lie, H. and Tognarelli, M.A. Experimental Investigation of Vortex-induced Vibration of Long Marine Risers. *Journal of Fluids and Structures* **2005**, *21*, 335-361.
9. Braaten, H. and Lie, H. NDP riser high mode VIV tests. Main Rerport No. 512394.00.01. *Norwegian Marine Technology Research Institue* **2004**.
10. Vortex induced vibration data repository. http://web.mit.edu/towtank/www/vivdr/datasets.html. *Center for Ocean Engineering, MIT.* **2007**.
11. Baarholm, G.S. and Larsen, C.M. and Lie, H. On Fatigue Damage Accumulation from In-line and Cross-flow Vortex-induced Vibrations on Risers. *Journal of Fluids and Structures* **2006**, *22*, 109-127.
12. Miner, M.A. Cumulative Damage in Fatigue. *Trans. ASME Journal of Applied Mechanics* **1945**, *12*, 159-164.
13. Matsuishi, M. and Endo, T. Fatigue of Metals Subjected to Varying Stress. *Japan Society of Mechanical Engineers* **1968**, Jukvoka, Japan.
14. Downing, S.D. and Socie, D.F. Simple Rainflow Counting Algorithms. *International Journal of Fatigue* **1982**, *4*, 31-40.
15. Bai, Y. and Bhattacharyya, R. and McCormick, M.E. Pipelines and Risers. *Elsevier Science Ltd.* **2001**.
16. Lie, H. and Kaasen, K.E. Modal Analysis of Measurements from A Large-scale VIV Model Test of A Riser in Linearly Sheared Flow. *Journal of Fluids and Structures* **2006**, *22*, 557-575.
17. Shi, C and Park, J and Manuel, L and Tognarelli, M.A. A Data-Driven Mode Identification Algorithm for Riser Fatigue Damage Assessment. *Journal of Offshore Mechanics and Arctic Engineering, Transactions of the ASME* **2014**, *136(3)*, 031702.
18. Mukundan, H. and Modarres-Sadeghi, Y. and Dahl, J.M. and Hover, F.S. and Triantafyllou, M.S. Monitoring VIV fatigue damage on marine risers. *Journal of Fluids and structures* **2009**, *25*, 617-628.
19. Mukundan, H. Vortex-induced Vibration of Marine Risers: Motion and Force Reconstruction from Field and Experimental Data. *Massachusetts Institute of Technology* **2008**, Cambridge, MA.
20. Kleiven, G. Identifying VIV Vibration Modes by Use of the Empirical Orthogonal Functions Technique. *21st International Conference on Offshore Mechanics and Arctic Engineering* **2002**, *Paper no. 28425*, Oslo, Norway.

21. Srivilairit, T. and Manuel, L. Vortex-induced Vibration and Coincident Current Velocity Profiles for a Deepwater Drilling Riser. *26th International Conference on Offshore Mechanics and Arctic Engineering* **2007**, *Paper no. 29596*, San Diego, USA.
22. Stoer, J. and Bulirsch, R. Introduction to numerical analysis. *New York: Springer, Third Edition* **2002**.
23. Press, W.H. and Teukolsky, S.A. and Vetterling, W.T. and Flannery, B.P. Numerical Recipes in C: The Art of Scientific Computing, Second Edition. *Cambridge University Press* **1992**.
24. Giacaglia, G.E.O. Trigonometric Interpolation. *Celestial Mechanics and Dynamical Astronomy* **1969**, *1*, 360-367.
25. Lucor, D. and Mukundan, H. and Triantafyllou, M.S. Riser Modal Identification in CFD and Full-scale Experiments. *Journal of Fluids and Structures* **2006**, *22*, 905-917.
26. Shi, C and Manuel, L and Tognarelli, M.A. and Botros, T. On the vortex-induced vibration response of a model riser and location of sensors for fatigue damage prediciton. *Journal of Offshore Mechanics and Arctic Engineering, Transactions of the ASME* **2012**, *134(3)*, 031802.
27. Shi, C and Manuel, L and Tognarelli, M.A. Empirical Procedures for Long-Term Prediction of Fatigue Damage for an Instrumented Marine Riser. *Journal of Offshore Mechanics and Arctic Engineering, Transactions of the ASME* **2014**, *136(3)*, 031402.